Available online at www.sciencedirect.com
ScienceDirect
Trans. Nonferrous Met. Soc. China 25(2015) 4151−4159
Transactions of Nonferrous Metals Society of China
www.tnmsc.cn

Dissolution kinetics and mechanism of gibbsitic bauxite and pure gibbsite in sodium hydroxide solution under atmospheric pressure

Hui-bin YANG[1,2], Xiao-lin PAN[1], Hai-yan YU[1], Gan-feng TU[1], Jun-min SUN[2]

1. School of Materials and Metallurgy, Northeastern University, Shenyang 110819, China;
2. Datang International High Aluminum Coal R&D Center (National Energy Sources High Aluminum Coal Development and Utilization Key Laboratory), Ordos 010321, China

Received 12 May 2015; accepted 12 October 2015

Abstract: The crystal structure, morphology, dissolution kinetics and mechanism of gibbsitic bauxite and pure gibbsite in NaOH solution under atmospheric pressure were systematically investigated by XRD and SEM. The results show that the size of single crystal of gibbsite in gibbsitic bauxite is smaller than that in pure gibbsite, but the interplanar distance is larger than that of pure gibbsite, which result in more defects in the crystal and less energy needed to dissolve in alkaline solution for the gibbsitic bauxite. The dissolution kinetic equations of gibbsitic bauxite and pure gibbsite were established, and the corresponding activation energies were calculated to be 99.144 and 115.149 kJ/mol, respectively.

Key words: gibbsite; crystal structure; dissolution; kinetics; Bayer process

1 Introduction

The Bayer process for the production of alumina involves bauxite digestion, solid−liquid separation, gibbsite precipitation and calcination, which has been widely investigated in the past decades. The gibbsitic bauxite, a natural mineral in the natural environment resulting from rock weathering, is the major raw materials for the Bayer process. The parent rocks appeared during the initial eruption of volcanoes. Most minerals come from parent rocks weathering [1]. The parent rocks of gibbsite are feldspar, plagioclase, mica and so on [1−3]. Gibbsite is formed during the process of chemical changes between weathering rocks and rainwater in hot and humid zones with long term potentially high rainfall and high leaching rates [3,4]. Different external environments result in various crystal structures and mineral compositions of gibbsite [3,5]. Most of gibbsitic bauxites belong to lateritic bauxite deposits, and the associated minerals are goethite and hematite [2,6]. During rock weathering process, the iron in the pyroxene becomes goethite at first, and then evolves to hematite. Hematite is the final mineral type of the iron-bearing mineral.

Pure gibbsite is $Al(OH)_3$, which is an intermediate product in the alumina production process. There are two processes to precipitate pure gibbsite, which are seed precipitation and carbonation decomposition. The precipitation process of $Al(OH)_3$ is one of the main technologies during the alumina process and was widely studied. BELAROUI et al [7] studied the agglomeration and growth phenomena of $Al(OH)_3$ crystal under different process conditions (seeding, mixing and impurities) by atomic force microscope [7]. LI et al [8,9] studied the kinetics and thermodynamics of the carbonation precipitation process and estimated the precipitation activation energy. WANG et al [10] studied different influencing factors of carbonation decomposition. LIU et al [11] and SAHU et al [12] studied the effect of soda content and additive on the precipitation process of $Al(OH)_3$. Pure gibbsite produced by seed precipitation has better crystal structure than that produced by carbonization precipitation, and the latter is easier to dissolve in the alkaline solution.

The dissolution process of bauxite is one of the main technologies during the Bayer process. PAN et al [13] and LI et al [14] studied the dissolution process

Foundation item: Projects (51104041, 51174054, 51374065) supported by the National Natural Science Foundation of China; Project (N130402010) supported by the Fundamental Research Funds for the Central Universities, China
Corresponding author: Xiao-lin PAN; Tel: +86-24-83686460; E-mail: panxl@smm.neu.edu.cn
DOI: 10.1016/S1003-6326(15)64065-1

of bauxite using bauxite and pure gibbsite, respectively. In most of the previous studies, the dissolution property of gibbsitic bauxite was investigated using pure gibbsite [15−21]. However, the gibbsitic bauxite and pure gibbsite are different in several aspects, such as crystal growth process, crystal structure and mineralization mode. Those differences will affect the dissolution property in the caustic soda solution. In this work, the dissolution kinetics and mechanism of gibbsitic bauxite and pure gibbsite produced by carbonization decomposition were systematically investigated in caustic soda solution under atmospheric pressure.

2 Experimental

2.1 Materials

The gibbsitic bauxite used in this work is from West Kalimantan of Indonesia. The sample size is between 0.20 and 0.50 mm, and the average particle size is 0.35 mm. The pure gibbsite used in the experiments is the product of carbonation decomposition. The particle size is between 0.08 and 0.15 mm and the average particle size is 0.11 mm. The gibbsitic bauxite sample was detected by the standard screens, while the pure gibbsite and red mud were detected by a laser nanometer size analyzer.

The particle size of sample for the chemical analysis and SEM is between 20 and 30 μm, and that for XRD analysis is less than 5 μm. The compositions of impurities in the pure gibbsite were detected by national or industry standard methods. The minerals were analyzed by the BRUKER X-ray diffraction using Cu target cathode. The voltage is 30 kV and the current is 15 mA. The scanning angle is 3° to 80°, and the step size is 0.02°. The alumina composition was analyzed by the EDTA titration method, and silica composition was analyzed by molybdenum blue photometric method. The compositions of iron, titanium dioxide and sodium oxide were analyzed by orthophenanthrolene spectrophotometry, diantipyrylmethane spectrophotometry and flame atomic absorption spectrometry, respectively.

The main chemical compositions of gibbsitic bauxite sample are shown in Table 1 and the mineral compositions are shown in Table 2. The main impurity contents of pure gibbsite are shown in Table 3. As shown in Table 1, the content of reactive silica is relatively low, which will result in low silica content in the digested solution. No desilication reaction will happen when the silica content is low. The dissolution experiments were performed under atmospheric pressure and the slurry was separated immediately after dissolution, which also limits the desilication reaction. The content of sodium oxide in the red mud is only 0.10% (mass fraction), and the corresponding alumina dissolution efficiency error is 0.05%. Therefore, for the sake of simplification, the effect of silica during the alumina dissolution process is not considered in this research.

Table 1 Chemical compositions of gibbsitic bauxite (mass fraction, %)

SiO_2	Fe_2O_3	Al_2O_3	TiO_2	Loss on ignition
3.55	24.07	43.24	2.71	24.67

Table 2 Mineral compositions in gibbsitic bauxite (mass fraction, %)

Gibbsite	Hematite	Goethite	Kaolinite	Quartz	Anatase
58.50	15.00	12.40	7.20	0.20	2.71

Table 3 Impurity contents of pure gibbsite (mass fraction, %)

Fe_2O_3	SiO_2	Na_2O	Loss on ignition
0.005	0.025	0.200	34.63

2.2 Methods

The dissolution conditions of pure gibbsite and gibbsitic bauxite are the same. The concentration of NaOH is 3 mol/L. When the ratio of liquid to solid is 10, the caustic ratio of the liquid after dissolution is approximately 5 if the dissolution efficiency of alumina of gibbsitic bauxite is 100%. When the caustic ratio of the liquid after dissolution is around 5, the estimated ratio of liquid to solid is 20 for the dissolution of pure gibbsite. Under these conditions, they have the same driving force in the dissolution process.

The water bath chamber with a single hole was selected for the experiments, and the temperature ranged from 30 to 100 °C. The mechanical stirring speed changed from 30 to 2000 r/min. The high pressure dissolution tests were carried out in an oil bath digester at 120 °C. The concentration of sodium oxide in the solution was analyzed by acid−base neutralization method. The concentration of alumina was detected by EDTA complexometry. The residues were washed using hot distilled water, and then dried for the analyses of XRD and SEM. The alumina dissolution efficiencies of the gibbsitic bauxite and pure gibbsite were calculated according to Eqs. (1) and (2), respectively.

$$\mu_A = \frac{w_1 c_0}{100 w_0 c_1} \tag{1}$$

$$\mu_A = \frac{w_1 c_0}{50 w_0 c_1} \tag{2}$$

where μ_A is the dissolution efficiency of alumina; w_0 is the content of alumina in the gibbsitic bauxite or pure gibbsite; w_1 is the concentration of alumina in sodium aluminate solution; c_0 and c_1 are the concentrations of NaOH before and after dissolution.

3 Results and discussion

3.1 Crystal structures of gibbsitic bauxite and pure gibbsite

The XRD patterns of the gibbsitic bauxite and pure gibbsite are shown in Figs. 1 and 2, respectively. As shown in Fig. 1, the gibbsitic bauxite mainly consists of gibbsite and several impurity minerals, such as kaolinite, quartz, hematite, goethite and anatase. As shown in Fig. 2, pure gibbsite is composed of aluminum hydroxide (α-$Al(OH)_3$).

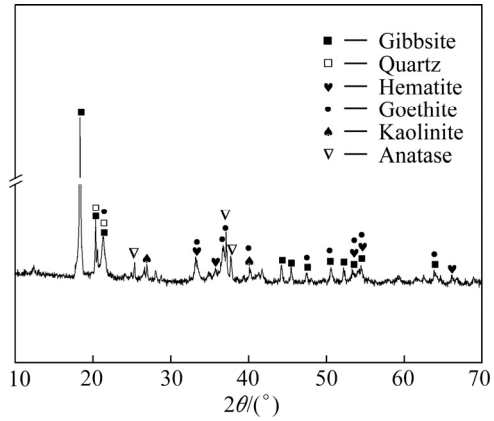

Fig. 1 XRD pattern of gibbsitic bauxite

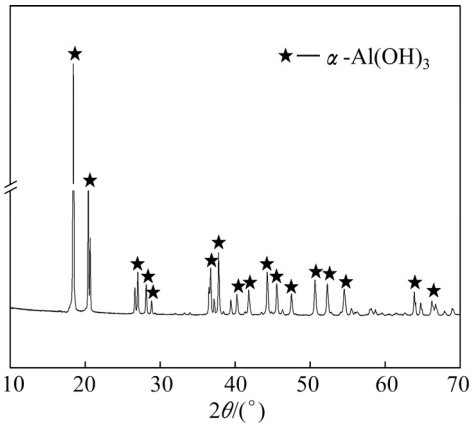

Fig. 2 XRD pattern of pure gibbsite

Pure gibbsite has a better crystal structure compared with the gibbsitic bauxite. All the 42 diffraction peaks perfectly fit with the standard card. In the range of 20°−70°, the peak heights (or intensity) of aluminum hydroxide are higher, which also indicates that the crystalline of pure gibbsite is better than that of gibbsitic bauxite. The crystal of gibbsitic bauxite has a poor crystallinity; even some characteristic peaks of the gibbsite are not shown in the pattern of the gibbsitic bauxite. The crystal structure with better crystallization is more stable. The crystallinity of gibbsitic bauxite is lower than that of pure gibbsite resulting in more defects in crystal structure and poor crystal morphology. The atom in the region of defects is more active than other atoms, which is easier to dissolute in the caustic soda solution.

According to the standard card of gibbsite, the interplanar distances of eight highest peaks were analyzed to compare the difference between gibbsitic bauxite and pure gibbsite. As shown in Table 4, no peak exists at 37.75° in the spectrum of gibbsitic bauxite.

The average of deviation rate of interplanar distance values was calculated according to Eq. (3):

$$\mu = \frac{d_x - d_0}{d_0} \times 100\% \tag{3}$$

where μ is the deviation rate of interplanar distance; d_x is the interplanar distance of the samples and d_0 is the interplanar distance of the standard card.

The deviation rates of interplanar distance values are given in Table 5. The interplanar distance of gibbsitic bauxite is larger than that of pure gibbsite, which indicates that the interatomic force of gibbsitic bauxite is weaker than that of pure gibbsite. Therefore, the activation energy of gibbsitic bauxite is smaller, which may result in easier dissolution and faster dissolution speed.

The SEM images of gibbsitic bauxite and pure gibbsite are shown in Figs. 3 and 4, respectively. Point *G* shown in Fig. 3(b) represents the gibbsite crystal,

Table 4 Interplanar distances of pure gibbsite and gibbsitic bauxite

2θ/(°)	Crystal orientation	Intensity/%	Interplanar distance/Å		
			Standard card	Pure gibbsite	Gibbsitic bauxite
18.27	(002)	100	4.85273	4.81961	4.85526
20.26	(110)	34.7	4.38004	4.34848	4.37865
20.50	(200)	17.3	4.32838	4.29873	4.33000
36.55	(021)	11.1	2.45634	2.44550	2.45563
37.61	(311)	16.3	2.38946	2.37852	2.38708
37.75	($\bar{2}$13)	9.7	2.38097	2.37919	–
44.09	($\bar{3}$13)	12.2	2.05211	2.04492	2.05105
50.45	($\bar{3}$14)	10.6	1.80738	1.80160	1.80569

Table 5 Deviation rates of interplanar distances of pure gibbsite and gibbsitic bauxite at different 2θ values

Sample	Deviation rate/%								
	18.27°	20.26°	20.50°	36.55°	37.61°	37.75°	44.09°	50.45°	Average
Pure gibbsite	−0.68	−0.72	−0.69	−0.44	−0.46	−0.07	−0.35	−0.32	−0.47
Gibbsitic bauxite	0.05	−0.03	0.04	−0.03	−0.10	−	−0.05	−0.09	−0.03

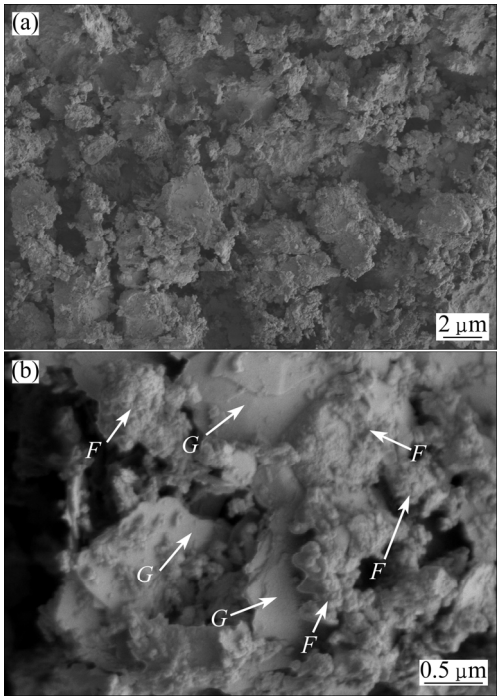

Fig. 3 SEM images of gibbsitic bauxite (*G*: Gibbsite; *F*: Hematite and goethite): (a) Holistic view; (b) Partial view

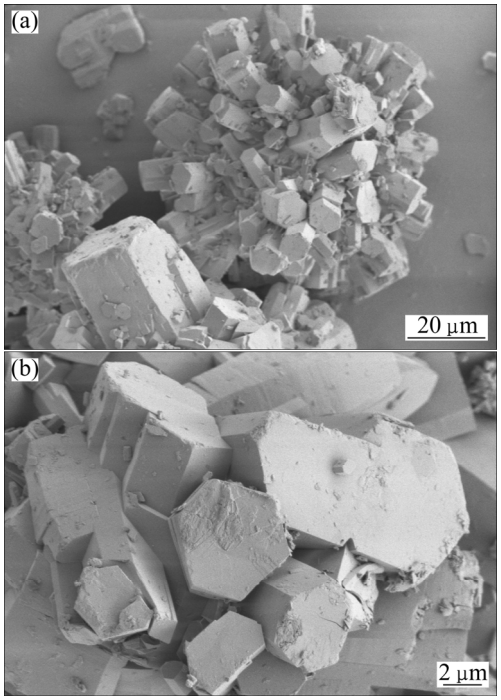

Fig. 4 SEM images of pure gibbsite: (a) Whole particle view; (b) Partial view

which is of sheet structure and wrapped by a layer of granular aggregates. The crystal size of the sheet structure is 2−3 μm. The minerals attaching on the structure of gibbsite are main hematite and goethite, which is shown by Point *F* in Fig. 3(b). The forms of the minerals containing iron in the gibbsitic bauxites are the same compared with most of the gibbsitic bauxite [6].

The SEM images of pure gibbsite are shown in Fig. 4. As shown in Fig. 4(a), the particles of pure gibbsite are of ball-like morphology with columnar branch crystals on the surface. Figure 4(b) shows that the columnar branch crystal surface is smooth, which indicates that it crystallizes well.

3.2 Dissolution property

The results of dissolution experiments are shown in Fig. 5. As shown in Fig. 5, the dissolution efficiency of the pure gibbsite is lower than that of gibbsitic bauxite under the same conditions. The dissolution efficiency of gibbsitic bauxite reaches above 75% when time is 20 min, while the dissolution efficiency of pure gibbsite is only 52.53%. The increase speed of the dissolution efficiency for gibbsitic bauxite is faster than that of pure gibbsite in the former 15 min. 15 min later, the growth speed of

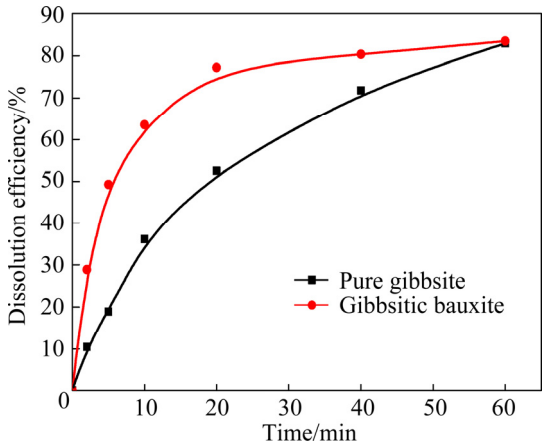

Fig. 5 Dissolution efficiency of gibbsitic bauxite and pure gibbsite at different time (Experiment condition: temperature 90 °C, stirring speed 350 r/min, NaOH concentration 3 mol/L)

the dissolution efficiency for gibbsitic bauxite decreases sharply, while that of pure gibbsite decreases gradually with the proceeding of the reaction. But the dissolution efficiency of the gibbsitic bauxite is always greater than that of pure gibbsite until the gibbsite dissolution process is almost finished.

The test results of different temperatures are shown

in Fig. 6 when the dissolution time is 30 min. As shown in Fig. 6, the dissolution efficiency of gibbsite is higher than that of pure gibbsite when the dissolution temperature is below 100 °C. Both of the dissolution efficiencies increase with the increase of temperature. The dissolution process of the gibbsitic bauxite is almost finished and the dissolution efficiency is 93.40% when the dissolution temperature is 120 °C, but the dissolution process of pure gibbsite has not finished and its dissolution efficiency is 94.67%.

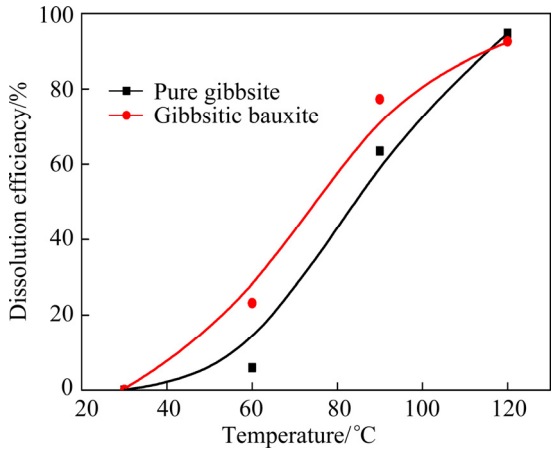

Fig. 6 Dissolution efficiencies of gibbsitic bauxite and pure gibbsite at different temperatures (Experiment condition: stirring speed 350 r/min, NaOH concentration 3 mol/L, dissolution time 30 min)

The SEM images and XRD pattern of the red mud are shown in Figs. 7 and 8. The SEM images of the residual particles, which are from the pure gibbsite in dissolution process, are shown in Fig. 9.

As shown in Fig. 7, the sheet structure, which belongs to gibbsite, disappears. The particle diameter of red mud is very small, mostly below 5 μm.

By comparing Fig. 8 with Fig. 1, it can be concluded that the dissolution of gibbsite and kaolinite is almost finished and no kaolinite is found in the red mud. The main minerals are goethite, hematite and other primary minerals. Few gibbsite and desilication product (DSP) are found in the red mud. The rest of few gibbsite may be wrapped by the layer of granular aggregates too tight to dissolve, but the amount is less so that the three highest diffraction peaks do not emerge completely.

The SEM images of the pure gibbsite residues when dissolution efficiency of gibbsite is 60% are shown in Fig. 9. The dissolution processes of well crystallized crystals, which grow from one single crystal nucleus, are well consistent with the shrinking nonporous model. The morphology of crystals is smooth after dissolution, which can be seen from the morphology of crystals shown in Fig. 9(a). The diameter of the crystal gradually decreases with the proceeding of the dissolution

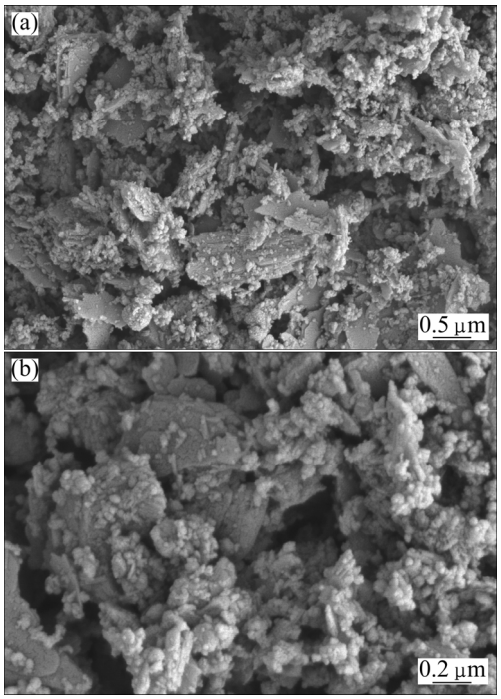

Fig. 7 SEM images of red mud: (a) Holistic view; (b) Partial view

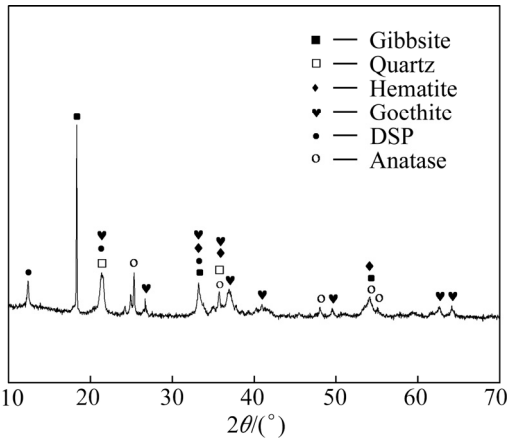

Fig. 8 XRD pattern of red mud

reactions. The morphology of dissolved gibbsite crystal is not smooth, because the velocity of reactions happening in the defects of the crystals is faster than that of other places. This indicates that agglomerations are in large amounts in the pure gibbsite of the carbonization decomposition. In the process of dissolution, most of the reactions happen along the agglomeration side, which makes the residue honeycomb-like, as shown in Fig. 9(b).

The particle size of gibbsitic bauxite is between 0.20 and 0.50 mm and the D_{50} is 0.35 mm, which is 2.11 times larger than that of pure gibbsite. But the dissolution speed of gibbsitic bauxite is still faster than that of pure gibbsite. The single crystal of gibbsite in the gibbsitic bauxite is 2−3 μm, which is much smaller than

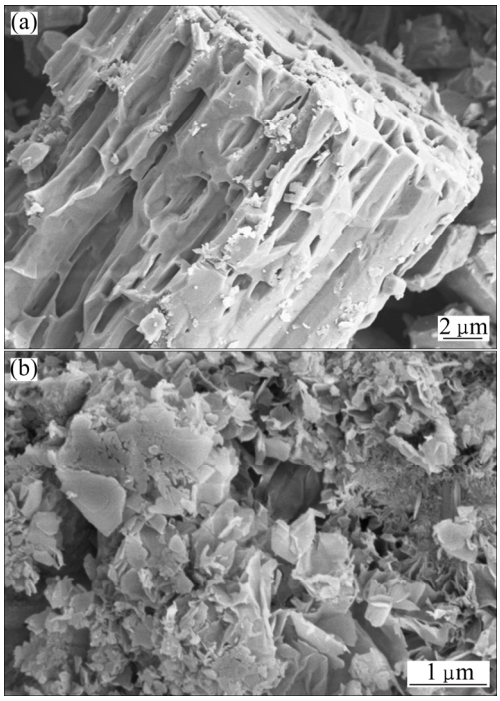

Fig. 9 SEM images of undissolved pure gibbsite: (a) Undissolved columnar branch crystals; (b) Undissolved aggregate particles

the particle size of bauxite. Other minerals, such as hematite and goethite attached on the surface of gibbsite crystals, make larger particle. The minerals attaching on the surface collapse into the solution during the dissolution reaction, which is reflected by the sludging phenomenon of red mud. The particle sizes of red mud are almost the same with each other when the dissolution temperatures reach 90 °C and 120 °C, respectively, which are less than 10 μm.

3.3 Dissolution kinetics

No solid products are produced during the dissolution process of pure gibbsite, which belongs to the simple liquid−solid reaction process. The process consists of three steps: The first step is the diffusion of liquid reactants towards the liquid−solid reaction surface by external diffusion; the second step is the reactions at the interface; the last step is the diffusion of products from the interface towards the liquid by internal diffusion. Previous researches [17,19] showed that the limiting step was diffusion rate or chemical reaction. As shown in Fig. 3, the gibbsite crystals are wrapped by a solid layer of granular aggregates. The existence of the solid layer may affect the dissolution process of bauxite and make the diffusion step the limiting step. The gibbsitic bauxite particle is nonporous and no new solid is produced during reaction, which accords with the shrinking nonporous models.

The dissolution kinetics equations are shown in Eqs. (4) and (5), when the reaction rates are controlled by the chemical reaction and solid layer, respectively [22,23]:

$$1-(1-\alpha)^{1/3}=kt \quad (4)$$

$$1-2\alpha/3-(1-\alpha)^{2/3}=kt \quad (5)$$

where α is the dissolution efficiency of Al_2O_3, k is the apparent rate constant of gibbsite and t is the dissolution time.

The dissolution experiments under different temperatures were carried out when the sample particle size was between 0.20 and 0.50 mm and the stirring speed was 350 r/min. The dissolution efficiency was calculated and used for Eqs. (4) and (5). The results are shown in Fig. 10. The linear relationships between $1-2\alpha/3-(1-\alpha)^{2/3}$ and t are better compared with those of $1-(1-\alpha)^{1/3}$ and t. This indicates that the reaction rate is mainly affected by the solid layer and the limiting step is diffusion. The values of R^2 (correlation coefficient) in Fig. 10(b) are higher than those of R^2 in Fig. 10(a). Therefore, the data in line with Eq. (5) are better, which also suggests that the dissolution of gibbsite is affected by the minerals attached on the gibbsite crystals.

The apparent rate constants (k) under different temperatures are shown in Table 6. The Arrhenius

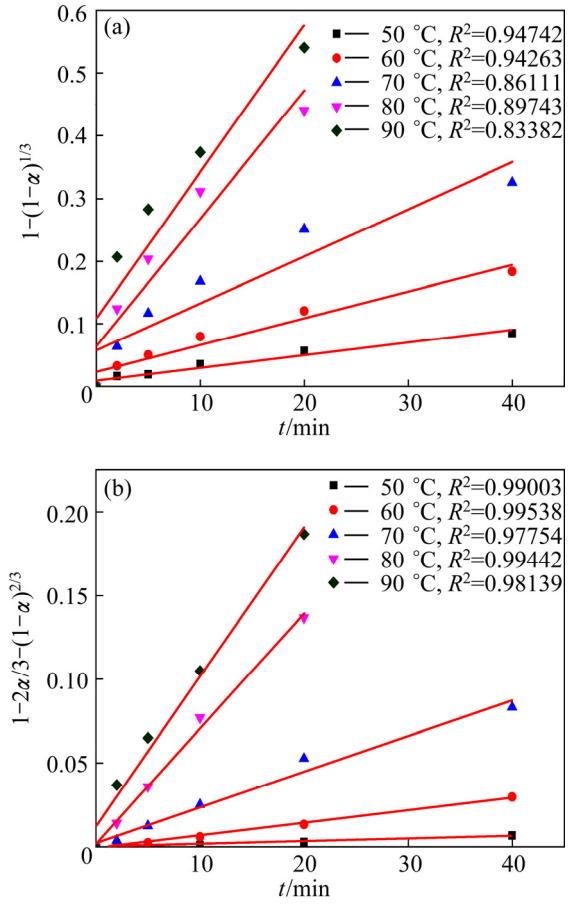

Fig. 10 Relation curves of $1-(1-\alpha)^{1/3}$ (a) and $1-2\alpha/3-(1-\alpha)^{2/3}$ (b) vs t for gibbsitic bauxite

Table 6 k values of gibbsitic bauxite

Temperature/°C	50	60	70	80	90
$k/10^{-4}\text{min}^{-1}$	1.73	7.47	21.20	69.00	89.00

equation is shown in Eq. (6). The Arrhenius curve of the dissolution process is shown in Fig. 11.

$$\ln k=-E/(RT)+\ln A \quad (6)$$

where k is the apparent rate constant of gibbsitic bauxite, E is the activity energy, R is the mole gas constant, T is the dissolution temperature and A is the preexponential factor.

The slope of the line in Fig. 11 is −11.93. According to Eq. (6), the activation energy of gibbsitic bauxite is 99.144 kJ/mol, which is close to the data calculated by JANAÍNA et al [17].

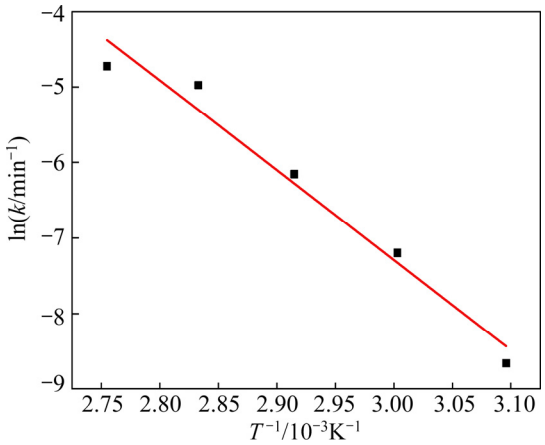

Fig. 11 Arrhenius curve of gibbsitic bauxite dissolution

According to the Arrhenius equation, shown as Eq. (6), A can be figured out. The average value of A is 2.42×10^{12} min^{-1}. The estimated dissolution kinetic equation of the gibbsitic bauxite is shown as:

$$1-2\alpha/3-(1-\alpha)^{2/3}=2.42\times10^{12}t\exp[-99144/(RT)] \quad (7)$$

The particle size of pure gibbsite was screened to between 75 and 150 μm in order to reduce the influence of grain size. The dissolution experiments of pure gibbsite were carried out under the same conditions with gibbsitic bauxite except for the liquid−solid ratio. The results are shown in Fig. 12. As shown in Fig. 12(a), the linear relationship between $1-(1-\alpha)^{1/3}$ and t is relatively perfect, and the values of R^2 are higher compared with those of Fig. 12(b). Therefore, the reaction rate is controlled by the chemical reaction. The values of k under different temperatures are shown in Table 7.

The Arrhenius curve of the dissolution process of pure gibbsite is shown in Fig. 13. The slope of the line is −13.85. According to the Arrhenius equation, the calculated activation energy of pure gibbsite is

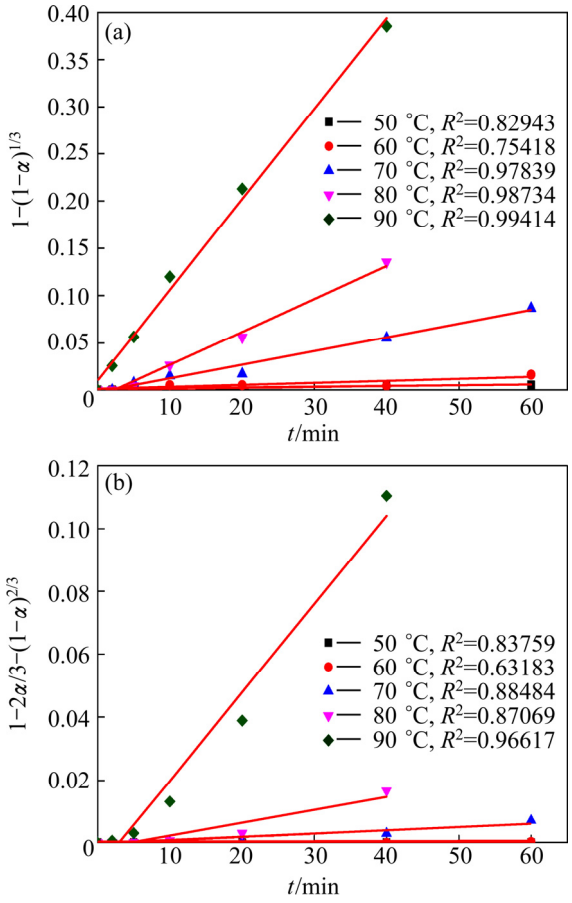

Fig. 12 Relation curves of $1-(1-\alpha)^{1/3}$ (a) and $1-2\alpha/3-(1-\alpha)^{2/3}$ (b) vs t for pure gibbsite

Table 7 k values of pure gibbsite dissolution

Temperature/°C	50	60	70	80	90
$k/10^{-4}\text{min}^{-1}$	1.04	2.22	14.40	34.80	95.90

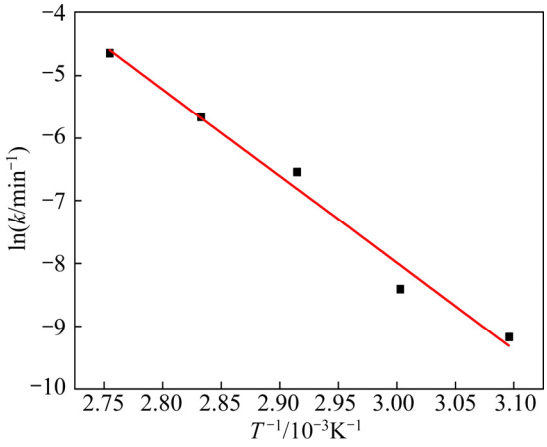

Fig. 13 Arrhenius curve of pure gibbsite dissolution

115.149 kJ/mol. It is very close to the data of 110 kJ/mol calculated by JANAÍNA et al [17]. The value of activation energy also indicates that the limiting step is the chemical reaction [23].

According to the Arrhenius equation, the calculated average value of A is 3.85×10^{14} min^{-1}. The estimated dissolution kinetic equation of the pure gibbsite is shown as:

$$1-(1-\alpha)^{1/3}=3.85\times10^{14}t\exp[-115149/(RT)] \quad (8)$$

The activation energy of pure gibbsite is higher than that of gibbsitic bauxite, which indicates that more energy is needed in the dissolution process of pure gibbsite. Therefore, the dissolution speed of pure gibbsite is lower than that of the gibbsitic bauxite.

4 Conclusions

1) The dissolution speed of pure gibbsite is lower than that of gibbsitic bauxite under atmospheric pressure in NaOH solution.

2) The crystallinity and size of single crystal of gibbsite in the gibbsitic bauxite are smaller than those in the pure gibbsite and the interplanar distance is larger than that of pure gibbsite.

3) The impurity minerals attached on the gibbsite crystals in the gibbsitic bauxite lower the gibbsite dissolution speed.

4) The dissolution kinetic equations of gibbsitic bauxite and pure gibbsite are $1-2\alpha/3-(1-\alpha)^{2/3}=2.42\times10^{12}t\exp[-99144/(RT)]$ and $1-(1-\alpha)^{1/3}=3.85\times10^{14}t\cdot\exp[-115149/(RT)]$, and the corresponding calculated activation energies are 99.144 and 115.149 kJ/mol, respectively.

References

[1] CERTINI G, WILSON M J, HILLIER S J, FRASER A R, DELBOS E. Mineral weathering in trachydacitic-derived soils and saprolites involving formation of embryonic halloysite and gibbsite at Mt. Amiata, Central Italy [J]. Geoderma, 2006, 133(3−4): 173−190.

[2] MULYANTO B, STOOPS G, van RANST E. Precipitation and dissolution of gibbsite during weathering of andesitic boulders in humid tropical West Java, Indonesia [J]. Geoderma, 1999, 89(3−4): 287−305.

[3] HERRMANN L, ANONGRAK N, ZAREI M, SCHULER U, SPOHRER K. Factors and processes of gibbsite formation in northern Thailand [J]. Catena, 2007, 71(2): 279−291.

[4] MUTAKYAHWA M K D, IKINGURA J R, MRUMA A H. Geology and geochemistry of bauxite deposits in Lushoto District, Usambara Mountains, Tanzania [J]. Journal of African Earth Sciences, 2003, 36(4): 357−369.

[5] EMIELDA Y, ROBERT G. Rehydration of heated gibbsite, kaolinite and goethite: An assessment of properties and environmental significance [J]. Applied Clay Science, 2012, 64: 61−74.

[6] SHEN Jian-guo, LIU Yun-hua, XU Jun-wen. Differences of mineralization of two gibbsitic bauxites in Guangxi Province [J]. Earth Science Frontiers, 1999, 6(S): s251−s256. (in Chinese)

[7] BELAROUI K, PONS M N, VIVIER H. Morphological characterisation of gibbsite and alumina [J]. Powder Technology, 2002, 127(3): 246−256.

[8] LI Xiao-bin, CHEN Bin, ZHOU Qiu-sheng, LIU Gui-hua, PENG Zhi-hong, LIU Xiang-min. Kinetics of carbonation decomposition of sodium aluminate solution [J]. The Chinese Journal of Nonferrous Metals, 2004, 14(5): 848−853. (in Chinese)

[9] LI Xiao-bin, LIU Xiang-min, GOU Zhong-ru, PENG Zhi-hong, LIU Gui-hua, ZHOU Qiu-sheng, DING An-ping, LI Ming, LIU Ye-xiang. Thermodynamics of carbonization of aluminate solution [J]. The Chinese Journal of Nonferrous Metals, 2003, 13(4): 1005−1010. (in Chinese)

[10] WANG Zhi, YANG Yi-hong, BI Shi-wen, XIE Yan-li. Influencing factors of sodium aluminate solution carbonation decomposition [J]. Nonferrous Metals, 2002, 54(1): 43−46. (in Chinese)

[11] LIU Gui-hua, WANG Peng, QI Tian-gui, LI Xiao-bin, TIAN Lü, ZHOU Qiu-sheng, PENG Zhi-hong. Variation of soda content in fine alumina trihydrate by seeded precipitation [J]. Transactions of Nonferrous Metals Society of China, 2014, 24(1): 243−249.

[12] SAHU N K, SARANGI C K, DASH B, TRIPATHY B C, SATPATHY B K, MEYRICK D, BHATTACHARYA I N. Role of hydrazine and hydrogen peroxide in aluminium hydroxide precipitation from sodium aluminate solution [J]. Transactions of Nonferrous Metals Society of China, 2015, 25(2): 615−621.

[13] PAN Xiao-lin, YU Hai-yan, DONG Kai-wei, TU Gan-feng, BI Shi-wen. Pre-desilication and digestion of gibbsitic bauxite with lime in sodium aluminate liquor [J]. International Journal of Minerals, Metallurgy and Materials, 2012, 19(11): 973−977.

[14] LI Xiao-bin, YAN Li, ZHAO Dong-feng, ZHOU Qiu-sheng, LIU Gui-hua, PENG Zhi-hong, YANG Shuai-shuai, QI Tian-gui. Relationship between $Al(OH)_3$ solubility and particle size in synthetic Bayer liquors [J]. Transactions of Nonferrous Metals Society of China, 2013, 23(5): 1472−1479.

[15] LI Xiao-bin, ZHAO Dong-feng, YANG Shuai-shuai, WANG Dan-qin, ZHOU Qiu-sheng, LIU Gui-hua. Influence of thermal history on conversion of aluminate species in sodium aluminate solution [J]. Transactions of Nonferrous Metals Society of China, 2014, 24(10): 3348−3355.

[16] LI Xiao-bin, YAN Li, ZHOU Qiu-sheng, LIU Gui-hua, PENG Zhi-hong. Thermodynamic model for equilibrium solubility of gibbsite in concentrated NaOH solutions [J]. Transactions of Nonferrous Metals Society of China, 2012, 22(2): 447−455.

[17] JANAÍNA A M P, MARCIO S, ENRICO D, JOSÉ C P, JOSÉ L F M, CRISTIANE A H. The kinetics of gibbsite dissolution in NaOH [J]. Hydrometallurgy, 2009, 96(1−2): 6−13.

[18] ADDAI-MENSAH J, DAWE J, RALSTON J. The dissolution and interactions of gibbsite particles in alkaline media [J]. Developments in Mineral Processing, 2000, 13: 1−7.

[19] BAO Li, ZHANG Ting-an, LIU Yan, DOU Zhi-he, LÜ Guo-zhi, WANG Xiao-min, MA Jia, JIANG Xiao-li. The most probable mechanism function and kinetic parameters of gibbsite dissolution in NaOH solution [J]. Chinese Journal of Chemical Engineering, 2010, 18(4): 630−634.

[20] YIN Ai-jun, CHEN Qi-yuan, ZHANG Ping-min. Studies on the kinetics of dissolution process of synthetic gibbsite by DSC [J]. Chemical Journal of Chinese Universities, 1991, 12 (11): 1507−1509. (in Chinese)

[21] LI Chao-qun, ZHANG Ping-min, CHEN Qi-yuan, CHEN Xin-min. Investigation of dissolution process kinetics of gibbsite [J]. Nonferrous Metals, 1991, 43(4), 52−55. (in Chinese)

[22] HUA Yi-xin. Introduction to metallurgical process dynamics [M]. Beijing: Metallurgical Industry Press, 2004. (in Chinese)

[23] LI Hong-gui. Hydrometallurgy [M]. Changsha: Central South University Press, 2005. (in Chinese)

三水铝石矿与纯三水铝石的常压碱溶动力学与溶出机理

杨会宾[1,2]，潘晓林[1]，于海燕[1]，涂赣峰[1]，孙俊民[2]

1. 东北大学 材料与冶金学院，沈阳 110819；
2. 大唐国际高铝煤炭研究开发中心(国家能源高铝煤炭资源开发利用重点实验室)，鄂尔多斯 010321

摘 要：结合 X 射线衍射和扫描电镜技术，对三水铝石矿与纯三水铝石的晶体结构和微观形貌进行对比，并对其在常压和 NaOH 溶液中的溶出动力学和溶出机理进行系统研究。结果表明，与纯三水铝石相比，铝土矿中三水铝石的单晶颗粒较小，而晶面间距较大。二者上述结构差异性导致矿石中三水铝石晶体缺陷较多，在碱溶液中溶解时需要克服的能量较低。建立三水铝石矿与纯三水铝石的溶出动力学方程，计算得到其溶出表观活化能分别为 99.144 和 115.149 kJ/mol。

关键词：三水铝石；晶体结构；溶解；动力学；拜耳法

(Edited by Wei-ping CHEN)